PHYS 414 Final Project: Stars, from Newton to Einstein

Enes Taha Göksu
Department of Physics, Koç University,
Rumelifeneri Yolu, 34450 Sariyer, Istanbul, Turkey
(Dated: January 11, 2026)

We study stellar structure across Newtonian gravity and general relativity, covering white dwarfs and neutron stars. In the Newtonian part, we derive the Lane–Emden equation for polytropic equations of state, obtain the mass identity and the mass–radius scaling, and use white dwarf observations to constrain the low-mass polytropic behavior. We then employ the full cold-degenerate electron equation of state to recover the full white dwarf mass–radius curve and the Chandrasekhar mass limit. In the relativistic part, we solve the Tolman–Oppenheimer–Volkoff (TOV) equations with a parametric relativistic polytropic equation of state for neutron stars, and analyze baryonic mass, binding energy, stability, the dependence of the maximum mass on the EOS parameter K, and the exterior solution for the metric function. All computational plots and numerical values are inserted as figures; numerical values can be added next to them.

NEWTON

(a) Lane–Emden equation

Hydrostatic equilibrium in Newtonian gravity for a spherically symmetric star is governed by

$$\frac{dm(r)}{dr} = 4\pi r^2 \rho(r), \tag{1}$$

$$\frac{dp(r)}{dr} = -\frac{Gm(r)\rho(r)}{r^2}. \tag{2}$$

We assume a polytropic equation of state (EOS)

$$p = K\rho^{\gamma} = K\rho^{1+1/n}, \tag{3}$$

where n is the polytropic index.

Step 1: eliminate $m(r)$. From Eq. (2),

$$\frac{1}{\rho}\frac{dp}{dr} = -\frac{Gm}{r^2}. \tag{4}$$

Differentiate and use Eq. (1):

$$\frac{d}{dr}\left(\frac{r^2}{\rho}\frac{dp}{dr}\right) = -G\frac{dm}{dr} = -4\pi G r^2 \rho. \tag{5}$$

Divide by r^2:

$$\frac{1}{r^2}\frac{d}{dr}\left(\frac{r^2}{\rho}\frac{dp}{dr}\right) + 4\pi G\rho = 0. \tag{6}$$

Step 2: introduce Lane–Emden variables. Using Eq. (3),

$$\frac{dp}{dr} = K\left(1+\frac{1}{n}\right)\rho^{1/n}\frac{d\rho}{dr}. \tag{7}$$

Define

$$\rho(r) = \rho_c \theta(\xi)^n, \qquad r = a\xi, \tag{8}$$

with

$$a^2 = \frac{K(n+1)}{4\pi G}\,\rho_c^{\frac{1-n}{n}}. \tag{9}$$

Substituting (8)–(9) into (6) cancels all dimensional quantities and yields the Lane–Emden equation

$$\frac{1}{\xi^2}\frac{d}{d\xi}\left(\xi^2\frac{d\theta}{d\xi}\right) + \theta^n = 0, \tag{10}$$

with regularity conditions $\theta(0) = 1$ and $\theta'(0) = 0$.

Series solution near the origin. To avoid the formal singularity of the $(2/\xi)\theta'$ term at $\xi = 0$, expand $\theta(\xi) = 1 + a_2\xi^2 + a_4\xi^4 + \cdots$. Plugging into Eq. (10) and matching powers gives

$$\theta(\xi) = 1 - \frac{\xi^2}{6} + \frac{n}{120}\xi^4 + \mathcal{O}(\xi^6), \tag{11}$$

which provides numerically stable initial data at small ξ.

Analytic solution for $n = 1$. For $n = 1$, Eq. (10) becomes linear:

$$\theta'' + \frac{2}{\xi}\theta' + \theta = 0. \tag{12}$$

Writing $\theta(\xi) = u(\xi)/\xi$ gives $u'' + u = 0$, so $u = A\sin\xi + B\cos\xi$. Regularity at $\xi = 0$ forces $B = 0$, and $\theta(0) = 1$ fixes $A = 1$, hence

$$\theta(\xi) = \frac{\sin\xi}{\xi}. \tag{13}$$

Mass identity and M–R scaling

The stellar surface is defined by the first zero ξ_n of θ: $\theta(\xi_n) = 0$, so $R = a\xi_n$. The total mass is

$$M = 4\pi\int_0^R r^2\rho(r)\,dr = 4\pi\rho_c a^3\int_0^{\xi_n}\xi^2\theta(\xi)^n\,d\xi. \tag{14}$$

A key identity follows directly from Eq. (10):

$$\frac{d}{d\xi}\left(\xi^2\theta'\right) = -\xi^2\theta^n \quad \Longrightarrow \quad \int_0^{\xi_n} \xi^2\theta^n d\xi = -\left[\xi^2\theta'(\xi)\right]_0^{\xi_n}. \tag{15}$$

Because $\theta'(0) = 0$, the lower limit vanishes and we obtain the standard mass formula

$$M = 4\pi\rho_c a^3\omega_n, \qquad \omega_n \equiv -\xi_n^2\theta'(\xi_n) > 0. \tag{16}$$

Using $R = a\xi_n$, this may also be written as

$$M = 4\pi\rho_c R^3\left(-\frac{\theta'(\xi_n)}{\xi_n}\right). \tag{17}$$

M–R scaling for fixed (K, n). From Eq. (9), $a \propto \rho_c^{(1-n)/(2n)}$ for fixed K, n, hence $R = a\xi_n \propto \rho_c^{(1-n)/(2n)}$ and, using Eq. (16), $M \propto \rho_c a^3 \propto \rho_c^{(3-n)/(2n)}$. Eliminating ρ_c gives

$$M \propto R^{\frac{3-n}{1-n}}. \tag{18}$$

(b) White dwarf observational data

The file `white_dwarf_data.csv` contains observational data for $N = 378$ white dwarfs, including their masses (in $M_\odot$) and surface gravities $\log_{10}(g)$ in CGS units. The stellar radius is obtained from

$$g = \frac{GM}{R^2} \quad \Longrightarrow \quad R = \sqrt{\frac{GM}{g}}. \tag{19}$$

The resulting sample spans the ranges $M \simeq 0.074$–$1.38\,M_\odot$ and $R \simeq 0.36$–$2.60\,R_\oplus$.

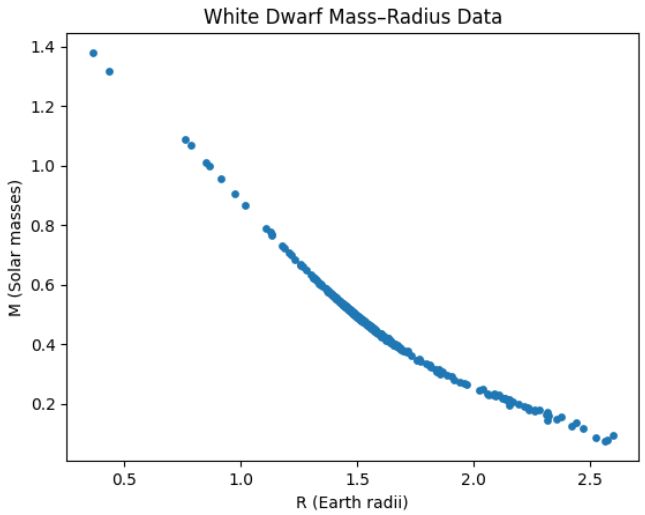

FIG. 1: Observed white dwarf mass–radius data.

(c) Low-mass WDs: effective polytrope and ρ_c

Introducing the relativity parameter $x = p_F/(m_e c)$, the pressure of a cold, degenerate electron gas is

$$P(x) = C\left[x(2x^2 - 3)\sqrt{1 + x^2} + 3\sinh^{-1} x\right], \tag{20}$$

while the mass density scales as

$$\rho(x) = D\,x^q. \tag{21}$$

For physical white dwarfs $q = 3$. In the nonrelativistic regime $x \ll 1$, expanding Eq. (20) yields

$$P(x) = \frac{8C}{5}\,x^5 + \mathcal{O}(x^7). \tag{22}$$

Using $x = (\rho/D)^{1/q}$, the EOS reduces to an effective polytrope,

$$P \simeq K_*\,\rho^{1+1/n_*}, \qquad n_* = \frac{q}{5-q}, \qquad K_* = \frac{8C}{5D^{5/q}}. \tag{23}$$

For $q = 3$ this gives $n_* = 3/2$, corresponding to $\gamma = 5/3$.

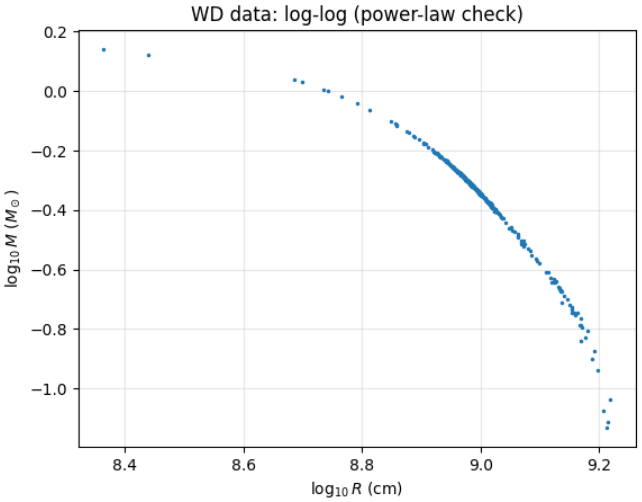

FIG. 2: White dwarf data in log–log scale.

A log–log fit of the low-mass subset yields a slope $s = -3.0$, consistent with the theoretical scaling $M \propto R^{-3}$ for $n_* = 3/2$, and an intercept $b = 26.68$ in $\ln M = \ln B + s \ln R$. From the fit we obtain

$$K_* = 2.79 \times 10^{12} \quad \text{(CGS units)}. \tag{24}$$

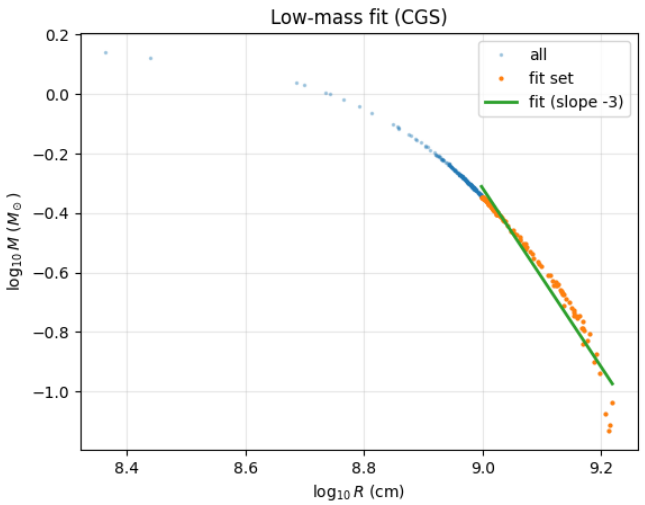

FIG. 3: Low-mass subset and log–log fit used to determine the polytropic index.

For $n_* = 3/2$, the Lane–Emden solution gives $\xi_{n_*} = 3.6538$ and $\omega_{n_*} = -\xi_{n_*}^2\,\theta'(\xi_{n_*}) = 2.7141$. The central density of each star in the low-mass sample follows from

$$\rho_c = \frac{M}{4\pi R^3}\left(-\frac{\theta'(\xi_{n_*})}{\xi_{n_*}}\right)^{-1}. \tag{25}$$

The inferred central densities lie in the range 6.7×10^4–$1.4 \times 10^6\,\mathrm{g\,cm^{-3}}$.

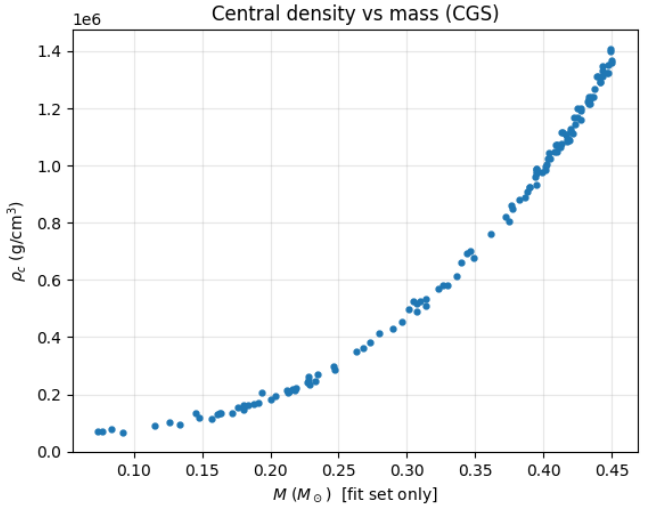

FIG. 4: Central density ρ_c versus mass for the low-mass white dwarf sample.

(d) Full WD EOS: fitting D using interpolation

With $q = 3$ fixed from the low-mass analysis, the full degenerate EOS depends on a single scale parameter D. For each trial value of D, we generate a theoretical $M(R)$ curve by sweeping the central density and compare it to all 378 observed white dwarfs via interpolation.

The theoretical expectation,

$$D_{\mathrm{theory}} = 7.79 \times 10^6, \tag{26}$$

is obtained from fundamental constants. The interpolation-based fit yields

$$D_{\mathrm{best}} = 7.44 \times 10^6, \qquad \frac{D_{\mathrm{best}}}{D_{\mathrm{theory}}} = 0.955, \tag{27}$$

corresponding to agreement at the few-percent level.

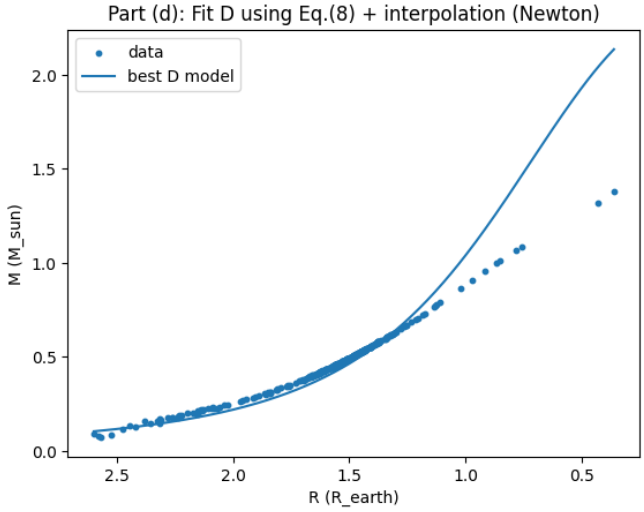

FIG. 5: Best-fit full EOS mass–radius curve compared to observational data.

(e) Full M–R curve and Chandrasekhar mass

Using the fitted EOS parameters, we compute the full white dwarf mass–radius relation by solving the Newtonian structure equations for 92 central density values. The resulting curve exhibits a maximum mass

$$M_{\mathrm{max}}^{(\mathrm{num})} = 1.4406\,M_\odot, \tag{28}$$

attained at a radius $R \simeq 0.170\,R_\oplus$.

In the ultrarelativistic limit $x \gg 1$, the EOS approaches a polytrope with $\gamma = 4/3$ ($n = 3$), leading to the Chandrasekhar mass

$$M_{\mathrm{Ch}}^{(\mathrm{theory})} = 1.4575\,M_\odot. \tag{29}$$

The numerical maximum satisfies

$$\frac{M_{\mathrm{max}}^{(\mathrm{num})}}{M_{\mathrm{Ch}}^{(\mathrm{theory})}} = 0.988, \tag{30}$$

demonstrating agreement with the analytic Chandrasekhar limit at the percent level.

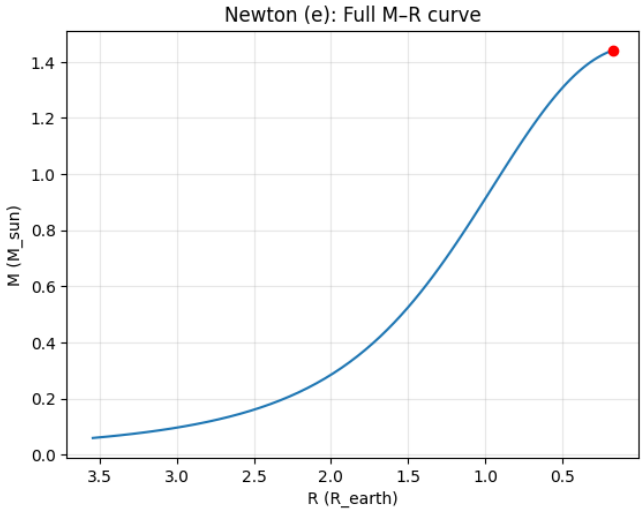

FIG. 6: Full white dwarf mass–radius curve with the Chandrasekhar mass indicated.

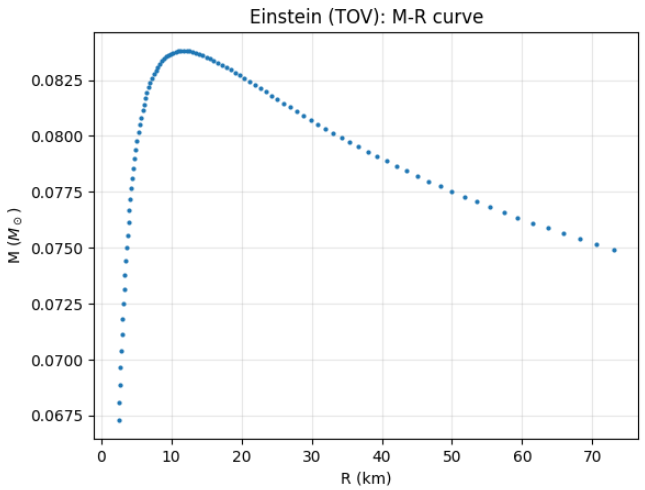

FIG. 7: Neutron star mass–radius curve obtained by sweeping the central pressure p_c.

EINSTEIN

We now model neutron stars in general relativity, using geometric units ($G = c = 1$) in the integration and converting to physical units in plots.

The EOS is given parametrically by

$$\begin{aligned} P &= K\rho_r^{\Gamma}, \\ \rho &= \rho_r + \frac{K}{\Gamma - 1}\rho_r^{\Gamma}, \end{aligned} \tag{31}$$

where ρ_r is the rest-mass energy density and ρ is the total energy density.

(a) TOV M–R curve

The Tolman–Oppenheimer–Volkoff (TOV) equations for a static, spherically symmetric perfect fluid are

$$\frac{dm}{dr} = 4\pi r^2 \rho, \tag{32}$$

$$\frac{dp}{dr} = -\frac{(m + 4\pi r^3 p)(\rho + p)}{r(r - 2m)}, \tag{33}$$

$$\frac{d\nu}{dr} = \frac{2(m + 4\pi r^3 p)}{r(r - 2m)}. \tag{34}$$

With $m(0) = 0$ and $p(0) = p_c$, we integrate outward until $p(R) = 0$ to define the stellar radius R and gravitational mass $M = m(R)$. Numerically, we start at a small $r = \epsilon$ using the regular expansion $m(r) \simeq (4\pi/3)\rho_c r^3$ to avoid the coordinate singularity at $r = 0$.

(b) Baryonic mass and binding energy

The baryonic mass counts rest mass integrated over the *proper* spatial volume. In Schwarzschild-like coordinates, the spatial line element contains $g_{rr} = (1 - 2m/r)^{-1}$, so the proper volume element is

$$dV_{\rm prop} = 4\pi r^2 \left(1 - \frac{2m}{r}\right)^{-1/2} dr. \tag{35}$$

Therefore,

$$\frac{dm_B}{dr} = 4\pi r^2 \rho_r \left(1 - \frac{2m}{r}\right)^{-1/2}, \tag{36}$$

and at the surface $M_B = m_B(R)$. The fractional binding energy is defined as

$$\Delta \equiv \frac{M_B - M}{M}, \tag{37}$$

so $\Delta > 0$ measures the mass deficit due to gravitational binding.

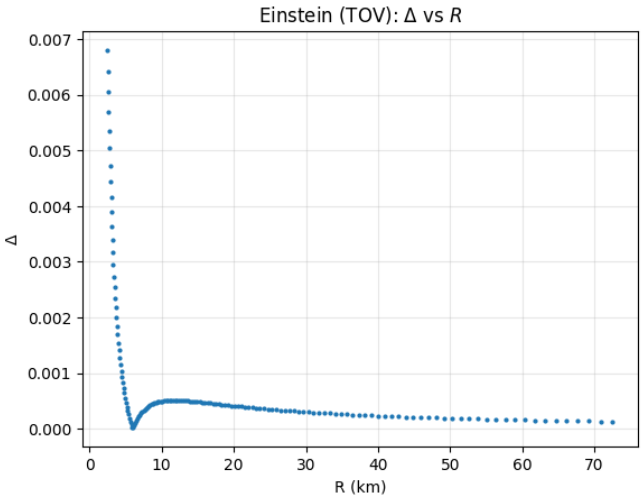

FIG. 8: Gravitational mass M versus baryonic mass M_B.

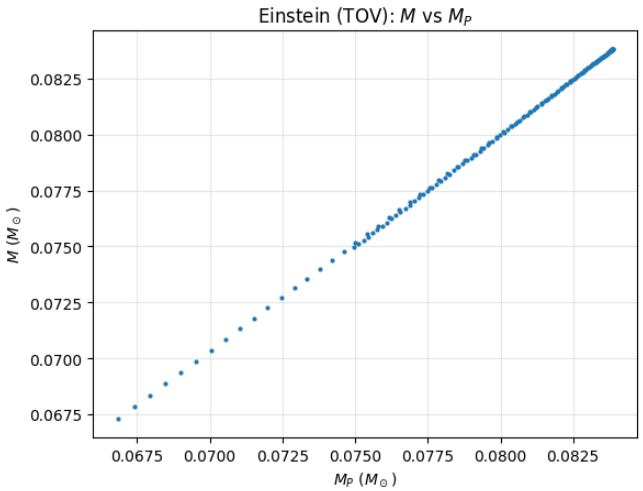

FIG. 9: Fractional binding energy $\Delta = (M_B - M)/M$ versus radius.

(c) Stability

Along a one-parameter sequence of equilibrium stars labeled by p_c (or ρ_c), the onset of the fundamental radial instability occurs at a turning point of the gravitational mass. A practical criterion is

$$\frac{dM}{d\rho_c} > 0 \;\Rightarrow\; \text{stable}, \qquad \frac{dM}{d\rho_c} < 0 \;\Rightarrow\; \text{unstable}. \tag{38}$$

In our discrete sequence we classify branches using the sign of dM/dp_c.

For the parameter choice used in Fig. 10, the sequence reaches a turning point at

$$M_{\max} = 0.0850\, M_\odot, \tag{39}$$
$$p_{c,\max} = 2.74 \times 10^{-5}, \tag{40}$$
$$R(M_{\max}) = 10.19 \text{ km}.$$

which marks the onset of instability within the turning-point criterion.

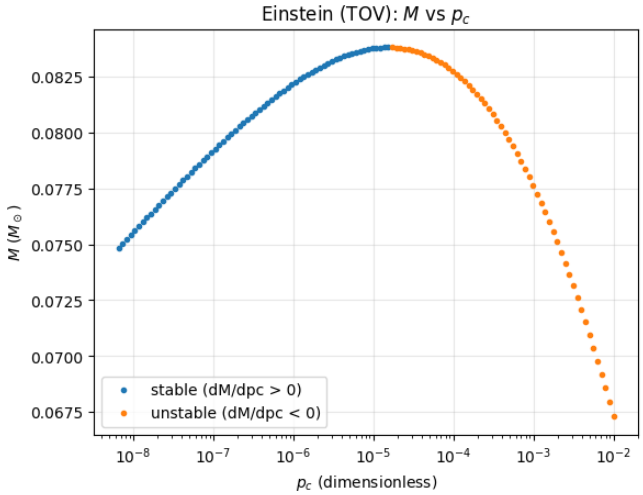

FIG. 10: M versus central pressure p_c with stable/unstable branches distinguished by the sign of dM/dp_c.

(d) $M_{\max}(K)$ and allowed K

Keeping Γ fixed and varying K changes the stiffness of the EOS. For each K in our scan, we compute a sequence $M(p_c)$, identify the maximum stable mass $M_{\max}(K)$ using the stability criterion in Sec. , and compare to the observational requirement

$$M_{\max}(K) \geq 2.5\, M_\odot. \tag{41}$$

For $\Gamma = 1.357$, no value of K in the scanned range reaches $2.5\, M_\odot$. For $\Gamma = 2.714$, the constraint is satisfied within our scan for

$$\frac{K}{K_0} \in [0.1,\, 10]. \tag{42}$$

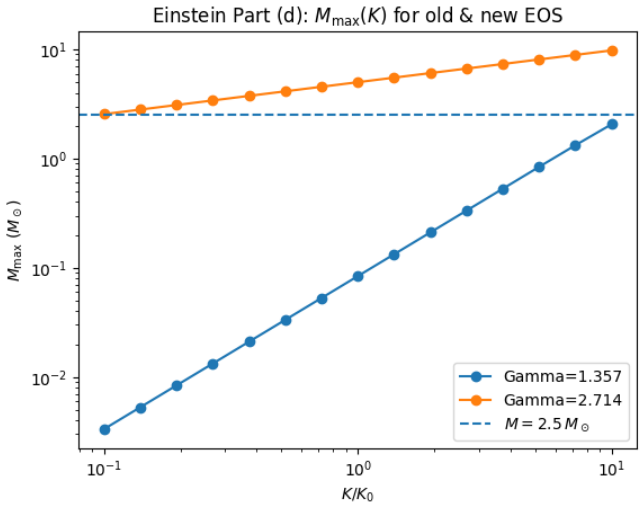

FIG. 11: Maximum stable mass $M_{\max}(K)$ for two EOS choices; dashed line shows $2.5\,M_\odot$.

(e) Exterior solution beyond the star

Outside the star ($r > R$), the pressure vanishes ($p = 0$), the energy density is zero ($\rho = 0$), and the enclosed mass is constant $m(r) = M$. The exterior spacetime is therefore Schwarzschild,

$$ds^2 = -e^{\nu(r)}dt^2 + \left(1 - \frac{2M}{r}\right)^{-1} dr^2 + r^2 d\Omega^2. \tag{43}$$

In the TOV system, the remaining metric equation is

$$\begin{aligned}\frac{d\nu}{dr} &= \frac{2\big(m + 4\pi r^3 p\big)}{r(r-2m)}, \\ &= \frac{2M}{r(r-2M)},\end{aligned} \tag{44}$$

valid for $r > R$ where $p = 0$ and $m(r) = M$.

Step 1: partial fractions. Write

$$\frac{2M}{r(r-2M)} = \frac{A}{r} + \frac{B}{r-2M}. \tag{45}$$

Multiplying by $r(r-2M)$ gives

$$2M = A(r-2M) + Br = (A+B)r - 2AM. \tag{46}$$

Matching coefficients yields $A+B = 0$ and $-2AM = 2M$, so

$$A = -1, \qquad B = 1, \tag{47}$$

hence

$$\frac{2M}{r(r-2M)} = -\frac{1}{r} + \frac{1}{r-2M}. \tag{48}$$

Step 2: integrate. Using the partial fraction decomposition in Eq. (48), we obtain

$$\begin{aligned}\nu(r) &= \int \left(-\frac{1}{r} + \frac{1}{r-2M}\right) dr \\ &= -\ln r + \ln(r-2M) + C \\ &= \ln\left(1 - \frac{2M}{r}\right) + C.\end{aligned} \tag{49}$$

Step 3: match at the surface. Continuity of $g_{tt} = -e^{\nu}$ at $r = R$ implies $\nu_{\text{out}}(R) = \nu_{\text{in}}(R) \equiv \nu(R)$, so from Eq. (49),

$$\nu(R) = \ln\left(1 - \frac{2M}{R}\right) + C \quad \Longrightarrow \quad C = \nu(R) - \ln\left(1 - \frac{2M}{R}\right). \tag{50}$$

Substituting back gives the exterior solution in matched form,

$$\nu(r) = \ln\left(1 - \frac{2M}{r}\right) - \ln\left(1 - \frac{2M}{R}\right) + \nu(R), \tag{51}$$

which is explicitly continuous at $r = R$.

CONCLUSION

In this project we investigated stellar structure from the Newtonian regime to general relativity, focusing on white dwarfs and neutron stars. In the Newtonian case, we derived the Lane–Emden equation for polytropic equations of state and showed that observational white dwarf data are consistent with the expected mass–radius behavior of a degenerate electron gas, including the Chandrasekhar mass limit. In the relativistic case, we solved the Tolman–Oppenheimer–Volkoff equations for neutron stars, examined global properties such as baryonic mass, binding energy, and stability, and studied how the maximum mass depends on the equation of state. Overall, the results illustrate how the interplay between the equation of state and gravity determines the global properties of compact stars.